Atomistic modeling of Co–Al compounds

Chuan-Hui Zhang,[a] Shuo Huang, Jiang Shen, and Nan-Xian Chen
Department of Physics, University of Science and Technology Beijing, 100083 Beijing, China

(Received 30 May 2013; accepted 13 August 2013)

The structural properties, the formation enthalpies, and the mechanical properties of Co–Al compounds (CoAl, $CoAl_3$, Co_3Al, Co_2Al_5, Co_2Al_9, and Co_4Al_{13}) are studied by using Chen's lattice inversion embedded-atom method. The potential is transferable and therefore does well for studying different Co–Al compounds. The calculated lattice parameters and cohesive energies are consistent with the experimental and theoretical results. The formation enthalpies of all the Co–Al compounds are negative; therefore, the chemical bonding between Co and Al atoms increases the stability of compounds. According to elastic constant restrictions, all the six Co–Al compounds are mechanically stable. CoAl alloy with the larger moduli and lower Poisson's ratio is the hard or brittle phase. Moreover, $CoAl_3$, Co_3Al, Co_2Al_5, and Co_2Al_9 alloys are considered to be ductile materials, which have lower ratio of shear modulus to bulk modulus.

I. INTRODUCTION

The Co–Al compounds attract great interests because of their importance in material science applications.[1–3] Many work about CoAl[4,5] and Co_4Al_{13},[6–8] which focus on sample preparation, structural analysis, and property measurement, has been done. Moreover, there were also some reports on $CoAl_3$,[9] Co_3Al,[10] Co_2Al_5,[11,12] and Co_2Al_9.[13]

The atomistic simulation could help people to understand more structural and physical properties of Co–Al compounds. In 1997, Vailhé and Farkas[14] calculated the crystal parameters, elastic constants, and bulk modules of three cubic structures (CoAl, $CoAl_3$, and Co_3Al)[14] by using embedded-atom method (EAM) potential. In 2002, Zhang et al.[15] applied modified analytic EAM (MAEAM) on CoAl and Co_3Al alloys. They found that the point defect types are Co antisite defects for the Co-rich side, and Al antisite defects for the Al-rich side in CoAl alloy. In addition, the self-diffusion behavior in Co_3Al happens at the first neighbor of the alloy, and diffusion elements are Co atoms. However, the above-mentioned two works did not simulate the hexagonal structure (Co_2Al_5) and monoclinic structures (Co_2Al_9 and Co_4Al_{13}). In 2007, Dong et al.[16] first utilized 2NN-MEAM (second nearest neighbor modified EAM) to the structural properties of uncubic Co–Al compounds. It is also found that the anisotropy in the γ/γ' (fcc-Co (γ) and Co_3Al (γ') phases) interfacial energy is relatively small and leaves a room for further modification by alloying with other elements. However, no systematic theoretical study has been reported on the mechanical properties of Co–Al compounds. It seems to be interesting to investigate their hardness, brittleness, and ductility by EAM calculations.

It is noteworthy that the interatomic pair potential can be strictly acquired to arbitrary-distance neighbor by using Chen's lattice inversion. In this paper, as many as six Co–Al compounds are systematically analyzed by Chen's lattice inversion embedded-atom method (CLI-EAM),[17,18] this is the first time to apply well transferable EAM potential to so many Co–Al compounds. Hence, one aim here is to verify the transferability of CLI-EAM potential, the other is to obtain comprehensive data of structural stability and mechanical properties of Co–Al compounds.

II. METHOD OF CALCULATION

A. Embedded-atom method

The basic equations of the embedded atom method are[19,20]

$$E_i(r) = F(\rho_i) + \frac{1}{2}\sum_{i\neq j}\Phi(r_{ij}) \quad , \tag{1}$$

$$\rho_i = \sum_{i\neq j} f(r_{ij}) \quad , \tag{2}$$

where $E_i(r)$ is the cohesive energy of each atom in metal, $F(\rho_i)$ is the energy to embed atom i in the background of the crystal, here ρ_i is the background electron density (BED) at atom i due to all other atoms, $\Phi(r_{ij})$ is the repulsive pair potential between atom i and atom j, $f(r_{ij})$ is the atomic electron density (AED) as a function of distance from the center.

In this paper, the formula of pair potential Φ is proposed to use the Morse function,[21]

[a]Address all correspondence to this author.
e-mail: chaorenhao2013@gmail.com
DOI: 10.1557/jmr.2013.255

 © Materials Research Society 2013

https://doi.org/10.1557/jmr.2013.255 Published online by Cambridge University Press

$$\Phi(r) = D_0(\exp[-2\alpha_0(r - r_0)] - 2\exp[-\alpha_0(r - r_0)]) \quad , \tag{3}$$

where r_0 is the nearest neighbor distance in the cell, D_0 and α_0 are the parameters for pair potential. The form of embedding energy F is proposed by Banerjea and Smith,[22] they put forward another form of embedding function based on effective medium theory[23] and universal energy function.[24] The details of pair potential and embedding energy are described in Sec. II. C. Meanwhile, the functions of BED and AED are both exponentially decrease forms:

$$F(\rho) = -F_0[1 - n\ln(\rho/\rho_e)](\rho/\rho_e)^n \quad , \tag{4}$$

$$\rho(r) = \rho_e \exp[-\lambda(r - r_0)] \quad , \tag{5}$$

$$f(r) = f_e \exp[-\beta(r - r_0)] \quad , \tag{6}$$

where all the parameters in Eqs. (4)–(6) are needed for fitting. Equation (5) is the analysis formula of BED. The parameters ρ_e and λ are obtained by fitting first-principles data. In another word, we calculated some BED points that change with lattice constants by using first-principles method, and then fitted these points with Eq. (5) to obtain the data of parameters ρ_e and λ. Equation (6) is the analysis formula of AED, and the parameters f_e and β are obtained by lattice inversion[25,26] method. More details of BED and AED are described in Sec. II. C.

B. Chen's lattice inversion

It is known that cohesive energy in crystal lattice $E(r)$ is a sum of interatomic pair potentials Φ', such as

$$E(r) = \frac{1}{2}\sum_{i\neq j}\Phi'(r_{ij}) = \frac{1}{2}\sum_{n=1}\Phi'(b_0(n)r_0) \quad , \tag{7}$$

where r_0 is the nearest neighbor distance, $b_0(n)$ is the ratio of the nth neighbor distance to the nearest neighbor distance. According to multiplicative semigroup, for any two integers m and n in semigroup $\{b(k)\}$, there always exists an integer l, such that

$$b(n)b(m) = b(l) \quad . \tag{8}$$

In other words, $\{b_0(k)\}$ can be replaced by $\{b(k)\}$. So Eq. (7) is equivalent to the following equation:

$$E(r) = \frac{1}{2}\sum_{n=1}^{\infty} r(n)\Phi'(b(n)r_0) \quad , \tag{9}$$

where $r(n)$ is the numbers of nth neighbor atoms, in which

$$r(n) = \begin{cases} r_0(b_0^{-1}[b(n)]) & b(n) \in \{b_0(n)\} \\ 0 & b(n) \notin \{b_0(n)\} \end{cases} \quad , \tag{10}$$

Therefore, pair potential Φ' is given by

$$\Phi'(r) = 2\sum_{n=1}^{\infty} I(n)E(b(n)r_0) \quad , \tag{11}$$

$$\sum_{b(k)|b(n)} I(k)r\left(b^{-1}[b(n)/b(k)]\right) = \delta_{n1} \quad . \tag{12}$$

The inversion coefficient $I(n)$ is structure dependent, such as fcc, bcc, and hcp metal.

As the same theory, Eq. (2) can written as,

$$\rho(r) = \sum_{n=1} r(n)f[b(n)r] \quad . \tag{13}$$

This form is important for the following discussion.

C. Chen's lattice inversion embedded atom method

For combination of EAM[17–20,27] and Chen's lattice inversion method,[25,26] the cohesive energy per atom of metal under homogeneous deformation is given by

$$E(r) = F[\rho(r)] + \frac{1}{2}\sum_{n=1}\Phi(b(n)r_0) \quad , \tag{14}$$

then

$$2\{E(r) - F[\rho(r)]\} = \sum_{n=1} r(m)\Phi[b(n)r_0] \quad , \tag{15}$$

$$\rho(r) = \sum_{n=1} r(n)f[b(n)r_0] \quad . \tag{16}$$

Therefore, the pair potential function and AED function can be acquired by Chen's lattice inversion[25,26]

$$\Phi(r) = 2\sum_{n=1} I(n)\{E[b(n)r_0] - F(\rho[b(n)r_0])\} \quad , \tag{17}$$

$$f(r) = \sum_{n=1} I(n)\rho(b(n)r_0) \quad . \tag{18}$$

The BED ρ in Eq. (18) can be obtained using first-principles calculations which were carried out with CASTEP code,[28] based on density functional theory (DFT). The cohesive energy, lattice constant, and bulk modulus of pure elements are input parameters (Table I). The Morse function of cohesive energy E in Eq. (18) can be obtained by fitting pure elements' experimental parameters.[29] The model parameters F_0 and n in the embedding Eq. (4) can be arbitrary initial value at the beginning.

https://doi.org/10.1557/jmr.2013.255 Published online by Cambridge University Press

TABLE I. The input experimental parameters of pure elements and the calculated parameters of Co–Al compounds.

Input experimental parameters				
	Cohesive energy (eV)	Lattice constant (Å)	Bulk modulus (GPa)	Elastic constant (GPa)
Al[29]	−3.39	2.8634	75.9	C_{11} = 106.8, C_{12} = 60.4, C_{44} = 288.3
Output	−3.38	2.8762	76.0	C_{11} = 102.1, C_{12} = 62.9, C_{44} = 293.3
Co[29]	−4.39	a = 2.507, c = 4.069	191	C_{11} = 295, C_{12} = 159, C_{13} = 111, C_{33} = 335, C_{44} = 71
Output	−4.40	a = 2.496, c = 4.063	189	C_{11} = 293, C_{12} = 149, C_{13} = 125, C_{33} = 317, C_{44} = 64

Calculated parameters									
	BED		AED		Embedding function		Pair potential		
	ρ_e (Å^{-3})	λ	f_e (Å^{-3})	β	n	F_0	D_0	α	r_0
Al	0.0194	7.275	0.00159	6.951	0.364	1.075	0.214	1.322	2.836
Co	0.0162	6.284	0.00128	6.250	0.56	3.04	0.227	2.150	2.476
Co–Al							0.220	1.686	2.650

Then the parameters are determined by the calculations that are compared between the experimental data in Table I. We obtained the data of pair interaction by inversion of the difference data between $E(r)$ and $F[(\rho(r))]$ in Eq. (15). And then we fitted these data of pair interaction with Morse formula to obtain three parameters D_0, α, and r_0. In addition, the data of $E(r)$ are from the experiment, the calculations of pure elements Al and Co are listed in Table I. It is seen that, the output results are consistent with the input experimental parameters. In CLI-EAM, the cutoff radii of fcc and hcp structures are larger than 8 Å, and the cutoff radius of the bcc structure is less than 3.5 Å, otherwise the phonon spectrum of these three structures would exit imaginary frequency. At the same time, the range which is larger than 10 Å or smaller than 2.0 Å is meaningless. Therefore, we chose 10 Å as the cutoff radius of Al and 3 Å as the cutoff radius of Co, respectively.

In binary alloy CLI-EAM, the cohesive energy E_c^{AB} of alloy is written as

$$E_c^{AB} = E_c^A + E_c^B + \Delta E \quad , \tag{19}$$

$$\Delta E = \sum_n r(n)\Phi_{AB}[b(n)r_0] \quad , \tag{20}$$

where E_c^A and E_c^B is the binding energy of metal A and B, respectively. The functions of them are both Eq. (1). The data of E_c^A, E_c^B, and E_c^{AB} come from experiment.[29–32] As people know, arbitrary N-body interaction energy term can be represented as sum of some pair interactions for pair potential model. Φ_{AB} is the pair potential between metal A and B. Based on Chen's lattice inversion,[25,26] Φ_{AB} is assumed to follow the formula,

$$\Phi_{AB} = \sum_n I(n)\Delta E[b(n)r_0] \quad , \tag{21}$$

where $I(n)$ is the inversion coefficient (the inversion coefficient bases on B2 structure here). This new-type EAM interatomic potential can be called the CLI-EAM potential; more details of CLI-EAM formalism have been published in the literature.[17,18,27] The input parameters for calculations are listed in Table I.

Because of using Chen's lattice inversion, the advantage of CLI-EAM over other EAM is that all the parameters can be obtained by first-principles calculation. Therefore, the problem of lack of experiments for pure metals is avoided, and the transferability of potential is enhanced.

D. Elastic constants and mechanics modulus

It is known that the elastic constants relating the various components of stress and strain are defined by,

$$C_{ij} = \frac{1}{V}\left(\frac{\partial^2 U}{\partial\varepsilon_i \partial\varepsilon_j}\right) \quad , \tag{22}$$

where V and U are the volume and the Helmholtz free energy of the crystal, ε is the strain tensor. The other mechanics modules are obtained by using Voigt, Reuss, and Hill (VRH) approximations.[33] All the elastic constants and structural properties were carried out with GULP code.[34] The bulk modulus (B) and shear modulus (G) are obtained from the elastic constants through Eqs. (23) and (24); Young's modulus (Y) and Poisson's ratio (ν) are obtained from the bulk modulus and shear modulus through Eqs. (25) and (26),

$$B = [2(C_{11} + C_{12} + 2C_{13}) + C_{33}]/9 \quad , \tag{23}$$

$$G = (7C_{11} - 5C_{12} + 2C_{33} + 12C_{44} - 4C_{13})/30 \quad , \tag{24}$$

$$Y = 9BG/(3B + G) \quad , \tag{25}$$

$$\nu = (3B - 2G)/2(3B + G) \quad . \tag{26}$$

https://doi.org/10.1557/jmr.2013.255 Published online by Cambridge University Press

III. RESULTS AND DISCUSSION

A. Structural properties

Based on phase diagrams, there are some Co–Al compounds confirmed in experiments, namely, CoAl, $CoAl_3$, Co_3Al, Co_2Al_5, Co_2Al_9, and Co_4Al_{13}. Although there are few available EAM potentials for all these compounds, the CLI-EAM alloy potential is utilized to calculate the lattice parameters, the formation enthalpies, and the cohesive energies of these compounds. The results are shown in Table II. It is seen that the calculated lattice constant of CoAl (2.867 Å) is consistent with the experiments of 2.863 Å[29] or 2.8608 Å.[30] This result is as good as 2NN-MEAM calculation of 2.86 Å[16] or EAM of 2.86 Å,[14] and the DFT results (2.862[35] and 2.867 Å[36]), and a little better than the result of MAEAM (2.961 Å[15]). The calculated cohesive energy of CoAl is −4.448 eV, that is also consistent with the EAM theoretical[14,16] and experimental results,[31] and a little better than DFT results (−4.505[4] and −4.393 eV[37]). In CLI-EAM method, the Morse function is used to describe the energy of crystal, so the acquired lattice constant and cohesive energy of CoAl are consistent with the experimental results.[29–31] Then we apply this alloy potential to the other Co–Al compounds. For two cubic structures $CoAl_3$ and Co_3Al, our results are as a similar conclusion to CoAl. For hexagonal structure Co_2Al_5, the results of lattice constant are a = 7.681 Å and c = 7.606 Å; it is a little larger than the results of 2NN-MEAM (a = 7.79 Å, c = 7.539 Å)[16] and experiment (a = 7.671 Å, c = 7.608 Å and a = 7.656 Å, c = 7.593 Å).[32,41] For monoclinic structures Co_2Al_9 and Co_4Al_{13}, our calculated lattice constants (a = 6.093 Å, b = 6.385 Å, and c = 8.652 Å) of Co_2Al_9 are consistent with the relevant experimental results[29,43] except Co_4Al_{13} (a = 15.547 Å, b = 7.679 Å, c = 12.465 Å) with a difference of 2.1–6.6% for experimental results.[44,45] From Table II, it can be seen that the results of Co_4Al_{13} by 2NN-MEAM also have the difference of 4.3–6.3%.[16] That means the calculations of lattice constants by EAM have the uncertainty. Moreover, EAM cannot describe the nonclose-packed crystal or

TABLE II. The calculated lattice parameters, enthalpy of formation (H_f), and cohesive energy (E_c) of Co–Al intermetallic compounds. Some results of first principles (DFT) and experiments (Exp.) are listed.

Compound	Method	Lattice parameters (Å)	E_c (eV)	H_f (eV)
CoAl	CLI-EAM	2.867	−4.448	−0.558
	EAM[14]	2.86	−4.47	...
	MAEAM[15]	2.961	−4.139	−0.249
	MEAM[16]	2.86	−4.45	−0.57
	DFT	a = 2.862,[35] a = 2.867[36]	−4.505[4] −4.393[37]	...
	Exp.	a = 2.8608,[30] a = 2.863[29]	−4.451[31]	−0.561[31]
$CoAl_3$	CLI-EAM	3.837	−3.987	−0.347
	EAM[14]	3.80	...	−0.34
	MEAM[16]	3.81	...	...
	DFT	3.73[37]	...	−0.43,[4] −0.402[38]
	Exp.[38]		...	−0.40
Co_3Al	CLI-EAM	3.657	−4.488	−0.348
	MAEAM[15]	3.644	−4.211	−0.071
	MEAM[16]	3.63	...	−0.28
	DFT	3.52,[37] 3.655[39]	...	−0.2[4]
	EAM[14]	3.56	...	...
Co_2Al_5	CLI-EAM	a = 7.681, c = 7.616	−3.893	−0.217
	MEAM[16]	a = 7.79, c = 7.539	...	−0.26
	DFT	a = 7.524[40]	...	−0.48,[4] −0.374[38] −0.69[40]
	Exp.	a = 7.671, c = 7.608[32] a = 7.656, c = 7.593[41]	...	−0.43[38]
Co_2Al_9	CLI-EAM	a = 6.093, b = 6.385, c = 8.652	−3.780	−0.208
	MEAM[16]	a = 6.13, b = 6.46, c = 8.42	...	−0.16
	DFT	a = 6.089[40]	...	−0.34,[4] −0.306[38] −0.32,[42] −0.46[40]
	Exp.	a = 6.149,[29] b = 6.290,[29] c = 8.557[29] a = 6.18,[43] b = 6.24,[43] c = 8.59[43]	... ...	−0.31,[38] −0.31[42] ...
Co_4Al_{13}	CLI-EAM	a = 15.547, b = 7.679, c = 12.465	−3.795	−0.170
	MEAM[16]	a = 15.72, b = 7.79, c = 12.14	...	−0.23
	DFT	...	...	−0.41[4]
	Exp.	a = 15.183,[44] b = 8.122,[44] c = 12.340[44] a = 14.79,[45] b = 8.14,[45] c = 12.72[45]	... ...	... ...

https://doi.org/10.1557/jmr.2013.255 Published online by Cambridge University Press

low-symmetry structures well. These differences may be attributed to the center-symmetry model of the CLI-EAM and the basic postulates of BED. In EAM model, BED is used to describe the many-body interactions. But people suppose it is a homogeneous electron gas in crystal.[19,20] Therefore, it can well describe high-symmetry structures such as cubic crystal but not direction effects in low-symmetry structures.

It is known that the cohesive energy can be used to describe the stability of the crystal; it is often defined as the total energy released by isolated atoms combined into solid. Hence, the larger the absolute value is, the more stable the crystal structure is. From Table II, the absolute values of cohesive energy of Co_2Al_5, Co_2Al_9, and Co_4Al_{13} are smaller than CoAl, which means CoAl is more energetically stable than the rest. Although our results are not as consistent with the experimental ones as some EAM calculations, our potential can well describe the structures and the energies of all the compounds with acceptable differences. As it is known, the transferability of potential is a very important character in atomic scale simulation, and therefore, the CLI-EAM potential has good transferability for Co–Al compounds.

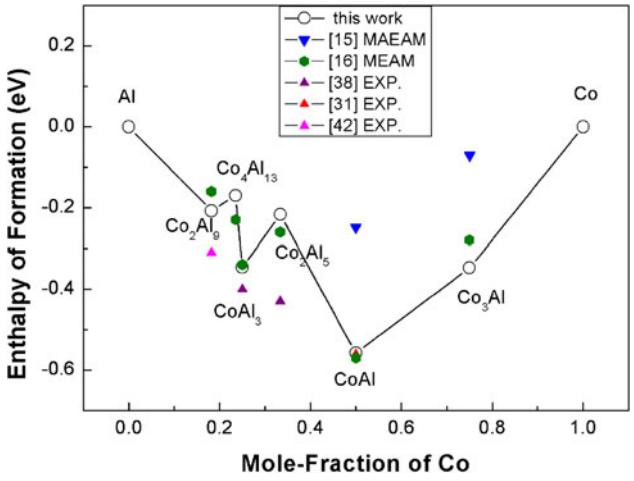


FIG. 1. Calculated enthalpies of formation for Co–Al compounds.

By studying the energies of optimized Co–Al compounds and metals Co and Al, the formation enthalpies (H_f) for Co–Al compounds were obtained. As shown in Table II, the calculated H_f of CoAl is −0.558 eV, it is consistent with 2NN-MEAM of −0.57 eV[16] and experimental results of −0.561 eV,[31] and a little better than the result of MAEAM (−0.249 eV).[15] All the results of Co–Al compounds are compared in Fig. 1, the values of H_f for $CoAl_3$, Co_3Al, Co_2Al_5, Co_2Al_9, and Co_4Al_{13} are −0.347, −0.348, −0.217, −0.208, and −0.170 eV, respectively. The absolute value of H_f first increases and then decreases when Co concentration increases, and it reaches maximum when the ratio of Co/Al concentration was 1:1. The negative H_f of Co–Al compounds means the chemical interactions between Co and Al atoms can increase the stability of compounds. Therefore all the Co–Al compounds are thermodynamically stable.

B. Elastic constants and mechanical properties

In this section, the elastic constants and the mechanical properties of Co–Al compounds are investigated by using the CLI-EAM alloy potential. All the results are shown in Table III together with the experimental[14] and the EAM calculation[15,16] results. Our calculated C_{11}, C_{12}, and C_{44} of CoAl are 275.9, 112.7, and 148.6 GPa respectively; they are similar to 2NN-MEAM of 265.9, 109.9, and 139.1 GPa[16] and experimental results of 269, 107, and 139 GPa,[14] and a little larger than the results of MAEAM (216.5, 136.4, and 90.6 GPa) and EAM (226, 146, and 115 GPa).[14,15] For cubic structures, the results of Co_3Al are as a similar conclusion to CoAl, although smaller differences exist for $CoAl_3$. The elastic constants of other uncubic structures

TABLE III. The calculated elastic properties (C_{ij} in GPa) of Co–Al intermetallic compounds.

Compound	Method	C_{11}	C_{12}	C_{13}	C_{22}	C_{23}	C_{33}	C_{44}	C_{55}	C_{66}	C_{15}	C_{25}	C_{35}	C_{46}
CoAl	CLI-EAM	275.9	112.7	...	...	...	...	148.6	...	...	...	...	...	...
	EAM[14]	226	146	...	...	...	...	115	...	...	...	...	...	...
	MAEAM[15]	216.5	136.4	...	...	...	...	90.6	...	...	...	...	...	...
	MEAM[16]	265.9	109.9	...	...	...	...	139.1	...	...	...	...	...	...
	Exp.[14]	269	107	...	...	...	...	139	...	...	...	...	...	...
Co_3Al	CLI-EAM	308.1	138.0	...	...	...	...	97.7	...	...	...	...	...	...
	MAEAM[15]	214.4	147.6	...	...	...	...	95.9	...	...	...	...	...	...
	MEAM[16]	313	144	...	...	...	...	142	...	...	...	...	...	...
	EAM[14]	280	184	...	...	...	...	131	...	...	...	...	...	...
$CoAl_3$	CLI-EAM	207.6	99.5	...	...	...	...	86.7	...	...	...	...	...	...
	MEAM[16]	182	85	...	...	...	...	69	...	...	...	...	...	...
	EAM[14]	251	151	...	...	...	...	94	...	...	...	...	...	...
Co_2Al_5	CLI-EAM	92.0	69.5	62.1	92.0	62.1	130.9	36.0	36.0	25.3	...	...	...	...
Co_2Al_9	CLI-EAM	109.5	55.2	58.1	158.9	42.0	117.7	38.9	31.2	33.9	17.4	7.8	5.7	9.2
Co_4Al_{13}	CLI-EAM	122.9	65.6	57.0	106.3	55.9	129.3	88.9	45.5	21.6	4.2	7.3	2.3	5.2

https://doi.org/10.1557/jmr.2013.255 Published online by Cambridge University Press

(Co_2Al_5, Co_2Al_9, and Co_4Al_{13}) are calculated; the results of corresponding elastic constants are smaller than the data of cubic structures.

As people know, the mechanical stability obeys the restrictions of elastic constants. Different structures have different restrictions. In the Co–Al system, CoAl, Co_3Al, and $CoAl_3$ are cubic structures; Co_2Al_9 and Co_4Al_{13} are monoclinic structures; Co_2Al_5 is a hexagonal structure. So here needs three restrictions.

For cubic structure, the restriction is[46]

$$C_{11} > 0, \quad C_{44} > 0, \quad C_{11} - C_{12} > 0, \quad C_{11} + 2C_{12} > 0 \quad . \tag{27}$$

And for monoclinic structure, the restriction is[47]

$$\begin{aligned} &C_{11} > 0, \quad C_{22} > 0, \quad C_{33} > 0, \quad C_{44} > 0, \quad C_{55} > 0, \quad C_{66} > 0, \\ &C_{11} + C_{22} + C_{33} + 2(C_{12} + C_{13} + C_{23}) > 0, \\ &\left(C_{11}C_{55} - C_{12}^2\right) > 0, \quad \left(C_{44}C_{66} - C_{46}^2\right) > 0, \quad C_{22} + C_{33} - 2C_{23} > 0, \\ &C_{22}\left(C_{33}C_{55} - C_{35}^2\right) + 2C_{23}C_{25}C_{35} - C_{23}^2C_{55} - C_{25}^2C_{33} > 0, \\ &2[C_{15}C_{25}(C_{33}C_{12} - C_{13}C_{23}) + C_{15}C_{35}(C_{22}C_{13} - C_{12}C_{23}) \\ &\quad + C_{25}C_{35}(C_{11}C_{23} - C_{12}C_{13})] \\ &\quad - \left[C_{15}^2\left(C_{11}C_{22} - C_{12}^2\right) + C_{55}\left(C_{11}C_{22}C_{33} - C_{11}C_{23}^2 - C_{22}C_{13}^2 - C_{33}C_{12}^2 + C_{12}C_{13}C_{23}\right)\right] > 0 \quad . \end{aligned} \tag{28}$$

For hexagonal structure, the restriction is[48]

$$C_{11} - |C_{12}| > 0, \quad (C_{11} + C_{12})C_{13} - 2C_{13}^2 > 0 \quad (C_{11} - C_{12})C_{44} - 2C_{14}^2 > 0 \quad . \tag{29}$$

From Table III, we find that all the elastic constants of the Co–Al compounds satisfy the above restrictions. That means they are all mechanically stable.

To better understand the mechanical properties of the Co–Al compounds, the bulk modulus B, the shear modulus G, the Young's modulus Y, and the Poisson's ratio ν are calculated and compared with the experimental[49] and the EAM results.[14,16] As shown in Table IV, our calculated bulk modulus of CoAl (167.1 GPa) is larger than the experimental (162 GPa)[49] and the MEAM (162 GPa)[16] data, whereas smaller than EAM (202).[14] The differences may be attributed to two reasons. One is that the defects in the materials are not considered in our calculations; another is that the effects of anisotropy on the elastic properties are not considered in experiments. To interpret our results, the bulk moduli of Co–Al compounds for different Co concentrations are shown in Fig. 2. As can be seen, the bulk modulus of metal Co is larger than metal Al, so the calculated bulk moduli of the compounds increase with increasing Co concentration except $CoAl_3$ (B = 135.5 GPa). The reason may be due to the effects of anisotropy of $CoAl_3$ lead to a little larger elastic constant, and then the larger elastic constant leads to a larger bulk modulus. In Table IV, CoAl has the highest shear modulus and Young's modulus, whereas Co_2Al_5 has the lowest values. Haines et al. proved that the hardness of a material is closely related to its shear modulus and

TABLE IV. The calculated bulk modulus (B), shear modulus (G), Young's modulus (Y), and Poisson's ratio (ν) of Co–Al intermetallic compounds.

Compound	Method	B (GPa)	G (GPa)	Y (GPa)	G/B	ν
CoAl	CLI-EAM	167.1	121.8	293.8	0.73	0.207
	EAM[14]	204	...	...	...	...
	MEAM[16]	162	...	...	...	...
	Exp.	162[14]	...	...	...	...
Co_3Al	CLI-EAM	194.7	92.6	239.8	0.47	0.295
	MEAM[16]	200	...	...	...	...
	EAM[14]	216	...	...	...	...
$CoAl_3$	CLI-EAM	135.5	47.1	126.6	0.34	0.344
	MEAM[16]	117	...	...	...	...
	EAM[14]	184	...	...	...	...
Co_2Al_5	CLI-EAM	105.6	24.7	68.7	0.23	0.392
Co_2Al_9	CLI-EAM	101.3	32.0	86.9	0.32	0.357
Co_4Al_{13}	CLI-EAM	106.9	54.3	139.3	0.51	0.283

https://doi.org/10.1557/jmr.2013.255 Published online by Cambridge University Press

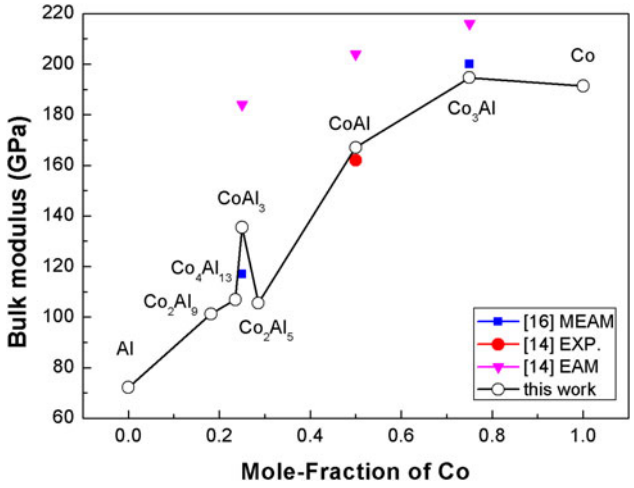


FIG. 2. Calculated bulk moduli of Co–Al compounds.

Young's modulus.[50] Although the relationships between the hardness and the modulus are not universal, it is generally recognized that the larger the modulus is, the higher hardness the material has. Therefore, CoAl with the largest modulus (G = 118.2 GPa, Y = 285.6 GPa) is the hard phase, whereas Co_2Al_5 with the smallest modulus (G = 24.7 GPa, Y = 68.7 GPa) is the soft phase. To study the brittleness and the ductility properties of the Co–Al compounds, the ratio of shear modulus to bulk modulus (G/B), which is an empirical criterion of the extent of fracture range of the material,[51] is studied. According to Table IV, $CoAl_3$, Co_3Al, Co_2Al_5, and Co_2Al_9 are ductile materials, which have lower G/B values of 0.34, 0.47, 0.23, and 0.32, respectively; whereas CoAl is a brittle material with a higher G/B value of 0.78. For Poisson's ratio, it is generally accepted that materials with low Poisson's ratio are brittle.[52,53] Thus, CoAl is a brittle material with a lower Poisson's ratio value of 0.207.

IV. SUMMARY

In this paper, the structural stability and the mechanical properties of Co–Al compounds (CoAl, $CoAl_3$, Co_3Al, Co_2Al_5, Co_2Al_9, and Co_4Al_{13}) were investigated by using CLI-EAM potential. The potential is transferable and therefore does well for studying different Co–Al compounds. The calculated lattice parameters and cohesive energies are consistent with the experimental and other EAM results. The formation enthalpies of all the Co–Al compounds are negative; therefore the chemical bonding between Co and Al atoms increase the stability of compounds. According to elastic constant restrictions, all the Co–Al compounds are mechanically stable. The bulk moduli of the compounds increase with the increasing Co concentration. Moreover, CoAl with the largest shear modulus and Young's modulus is the hard phase, and Co_2Al_5 with the smallest modulus is the soft phase. $CoAl_3$, Co_3Al, Co_2Al_5, and Co_2Al_9 with lower B/G values are considered to be ductile materials, and CoAl with a lower Poisson's ratio value of 0.207 is a brittle material.

ACKNOWLEDGMENT

This work was supported in part by the National Basic Research Program of China under Grant No. 2011CB606400.

REFERENCES

1. W. Steurer: Twenty years of structure research on quasicrystals. Part I. Pentagonal, octagonal, decagonal and dodecagonal quasicrystals. *Z. Kristallogr.* **219**, 391 (2004).
2. F. Fleischer, T. Weber, D.Y. Jung, and W. Steurer: σ-$Al_{13}Co_4$, a new quasicrystal approximant. *J. Alloys Compd.* **500**, 153 (2010).
3. M. Heggen, D.W. Deng, and M. Feuerbacher: Plastic deformation properties of the orthorhombic complex metallic alloy phase $Al_{13}Co_4$. *Intermetallics* **15**, 1425 (2007).
4. M. Mihalkovič and M. Widom: First-principles calculations of cohesive energies in the Al-Co binary alloy system. *Phys. Rev. B* **75**, 014207 (2007).
5. M. Mizuno, H. Araki, and Y. Shirai: Energetics and structural relaxation of constitutional defects in CoAl and CoTi from first principles. *Phys. Rev. B* **68**, 144103 (2003).
6. C. Bergman, C. Girardeaux, C. Perrin-Pellegrino, P. Gas, D. Chatain, J.M. Dubois, and N. Rivier: Wetting of decagonal $Al_{13}Co_4$ and cubic AlCo thin films by liquid Pb. *Philos. Mag.* **86**, 849 (2006).
7. M. Heggen, L. Houben, and M. Feuerbacher: Metadislocations in the structurally complex orthorhombic alloy $Al_{13}Co_4$. *Philos. Mag.* **88**, 2333 (2008).
8. J. Dolinšek, M. Komelj, P. Jeglič, S. Vrtnik, D. Stanić, P. Popčević, J. Ivkov, A. Smontara, Z. Jagličić, and P. Gille: Anisotropic magnetic and transport properties of orthorhombic $Al_{13}Co_4$. *Phys. Rev. B* **79**, 184201 (2009).
9. H-Z. Luo, Z-Y. Zhu, L. Ma, S-F. Xu, G-H. Wu, H-Y. Liu, J-P. Qu, Y-X. Li, X-X. Zhu, C-B. Jiang, and H-B. Xu: Effect of Cr on the electronic structure of Co_3Al intermetallic compound: A first-principles study. *J. Magn. Magn. Mater.* **320**, 1345 (2008).
10. V.K. Portnoi, K.V. Tretyakov, and V.I. Fadeeva: Structural transformations during the mechanochemical synthesis and heating of Co-Al Alloys. *Inorg. Mater.* **40**, 937 (2004).
11. G.V. Golubkova, O.I. Lomovsky, Y.S. Kwon, A.A. Vlasov, and A.L. Chuvilin: Formation of nanocrystalline structures in a Co-Al system by mechanical alloying and leaching. *J. Alloys Compd.* **351**, 101 (2003).
12. A. Ormeci and Y. Grin: Chemical bonding in Al_5Co_2: The electron localizability-electron density approach. *Isr. J. Chem.* **51**, 1349 (2011).
13. V.K. Portnoi, K.V. Tretyakov, V.I. Fadeeva, and J. Latuch: Effects of liquid quenching and subsequent heating on the structure of Co-Al Alloys. *Inorg. Mater.* **41**, 350 (2005).
14. C. Vailhé and D. Farkas: Shear faults and dislocation core structures in B2 CoAl. *J. Mater. Res.* **12**, 2559 (1997).
15. B-W. Zhang, W-Y. Hu, and X-L. Su: *Theory of Embedded Atom Method and its Application to Materials Science-atomic Scale Materials Design Theory* (Hunan University Press, Hunan, China, 2003), p. 397.
16. W-P. Dong, H-K. Kim, W-S. Ko, B-M. Lee, and B-J. Lee: Atomistic modeling of pure Co and Co-Al system. *Calphad* **38**, 7 (2012).

https://doi.org/10.1557/jmr.2013.255 Published online by Cambridge University Press

17. C-H. Zhang, J-J. Han, S. Huang, and J. Shen: Chen's lattice inversion embedded-atom method for FCC metal. *Adv. Mater. Res.* **320**, 415 (2011).
18. C-H. Zhang, S. Huang, J. Shen, and N-X. Chen: Chen's lattice inversion embedded-atom method for Ni-Al alloy. *Chin. Phys. B* **21**, 113401 (2012).
19. M.S. Daw and M.I. Baskes: Semiempirical, quantum mechanical calculation of hydrogen embrittlement in metals. *Phys. Rev. Lett.* **50**, 1285 (1983).
20. M.S. Daw and M.I. Baskes: Embedded-atom method: Derivation and application to impurities, surfaces, and other defects in metals. *Phys. Rev. B* **29**, 6443 (1984).
21. P.M. Morse: Diatomic molecules according to the wave mechanics II. Vibrational levels. *Phys. Rev.* **34**, 57 (1929).
22. A. Banerjea and J.R. Smith: Origins of the universal binding-energy relation. *Phys. Rev: B, Condens. Matter* **37**, 6632 (1988).
23. J.K. Norskov and N.D. Lang: Effective-medium theory of chemical binding: Application to chemisorptions. *Phys. Rev. B* **21**, 2131 (1980).
24. J.H. Rose, J.R. Smith, F. Guinea, and J. Ferrante: Universal features of the equation of state of metals. *Phys. Rev. B* **29**, 2963 (1984).
25. N-X. Chen: Modified mobius inverse formula and its applications in physics. *Phys. Rev. Lett.* **64**, 1193 (1990).
26. N-X. Chen, Z-D. Chen, and Y-C. Wei: Multidimensional inverse lattice problem and a uniformly sampled arithmetic fourier transform. *Phys. Rev. E* **55**, R5 (1998).
27. S. Huang, C-H. Zhang, J. Sun, Y-P. Li, Z-F. Zhang, and J. Shen: Formation and migration mechanism of the vacancy in three typical structures metal. *Appl. Phys.* **2**, 50 (2012).
28. M.D. Segall, P.J.D. Lindan, M.J. Probert, C.J. Pickard, P.J. Hasnip, S.J. Clark, and M.C. Payne: First-principles simulation: Ideas, illustrations and the CASTEP code. *J. Phys: Condens. Matter* **14**, 2717 (2002).
29. P. Villars and L. Calvert: *Pearson's Handbook Desk Edition: Crystallographic Data for Intermetallic Phases*, 2nd ed. (ASM International, Materials Park, OH, 1997), p. 135.
30. M.J. Cooper: An investigation of the ordering of the phases CoAl and NiAl. *Philos. Mag.* **8**, 805 (1963).
31. R. Hultgren, P. Desai, D. Hawkins, N. Gleiser, and K. Kelly: *Selected Values of Thermodynamic Properties of Binary Alloys* (ASM International, Materials Park, OH, 1973), p. 214.
32. Н.П. ЛЯКИШЕВ: *Handbook of Binary Alloy Phase Diagrams* (Beijing Chemical Industry Press, Beijing, China, 2009), p. 52.
33. O.L. Anderson: A simplified method for calculating the debye temperature from elastic constants. *J. Phys. Chem. Solids* **24**, 909 (1963).
34. J.D. Gale and A.L. Rohl: The general utility lattice program. *Mol. Simul.* **29**, 291 (2003).
35. M.J. Mehl, J.E. Osburn, D.A. Papaconstantopoulos, and B.M. Klein: Structural properties of ordered high-melting-temperature intermetallic alloys from first-principles total-energy calculations. *Phys. Rev. B* **41**, 10311 (1990).
36. M.F. Grosso, H.O. Mosca, and G. Bozzolo: Thermal and physical properties of B2 Al-Ir-X (X = Ni, Ru, Pd, Co, Fe) alloys. *Intermetallics* **18**, 945 (2010).
37. H. Ohtani, M. Yamano, and M. Hasebe: Thermodynamic analysis of the Co-Al-C and Ni-Al-C systems by incorporating ab initio energetic calculations into the CALPHAD approach. *Calphad* **28**, 177 (2004).
38. M. Widom and J.A. Moriarty: First-principles interatomic potentials for transition-metal aluminides. II. Application to Al-Co and Al-Ni phase diagrams. *Phys. Rev. B* **58**, 8967 (1998).
39. S.R. Broderick, H. Aourag, and K. Rajan: Data mining density of states spectra for crystal structure classification: An inverse problem approach. *Stat. Anal. Data Min.* **1**, 353 (2009).
40. G. Trambly de Laissardiere, D. Nguyen Manh, L. Magaud, J.P. Julien, F. Cyrot-Lackmann, and D. Mayou: Electronic structure and hybridization effects in hume-rothery alloys containing transition elements. *Phys. Rev. B* **52**, 7920 (1995).
41. J.B. Newkirk, P.J. Balck, and A. Damjanovic: The refinement of the Co_2Al_5 structures. *Acta Crystallogr.* **14**, 532 (1961).
42. J.A. Moriarty and M. Widom: First-principles interatomic potentials for transition-metal aluminides: Theory and trends across the 3d series. *Phys. Rev. B* **56**, 7905 (1997).
43. X-L. Ma and K-H. Kuo: Decagonal quasicrystal and related crystalline phases in slowly solidified Al-Co alloys. *Metall. Mater. Trans. A* **23**, 1121 (1992).
44. R.C. Hudd and W.H. Taylor: The structure of Co_4Al_{13}. *Acta Crystallogr.* **15**, 441 (1962).
45. J. Grin, U. Burkhardt, M. Ellner, and K. Peters: Crystal structure of orthorhombic Co_4Al_{13}. *J. Alloys Compd.* **206**, 243 (1994).
46. J.F. Nye: *Physical Properties of Crystals* (Oxford University Press, Oxford, England, 1985), p. 85.
47. O. Beckstein, J.E. Klepeis, G.L.W. Hart, and O. Pankratov: First-principles elastic constants and electronic structure of α-Pt2Si and PtSi. *Phys. Rev. B* **63**, 134112 (2001).
48. T. Tsuchiya, T. Yamanaka, and M. Matsui: Molecular dynamics study of pressure-induced transformation of quartz-type GeO_2. *Phys. Chem. Miner.* **27**, 149 (2000).
49. R.L. Fleischer: Substitutional solutes in AlRu-I. Effects of solute on moduli, lattice parameters and vacancy production. *Acta Metall. Mater.* **41**, 863 (1993).
50. J. Haines, J.M. Leger, and G. Bocquillon: Synthesis and design of superhard materials. *Annu. Rev. Mater. Res.* **31**, 1 (2001).
51. S.F. Pugh: XCII. Relations between the elastic moduli and the plastic properties of polycrystalline pure metals. *Philos. Mag.* **45**, 823 (1954).
52. J. Schroers and W.L. Johnson: Ductile bulk metallic glass. *Phys. Rev. Lett.* **93**, 255506 (2004).
53. K. Gschneidner, A. Russell, A. Pecharsky, J. Morris, Z. Zhang, T. Lograsso, D. Hsu, C.H. Lo, Y. Ye, A. Slager, and D. Kesse: A family of ductile intermetallic compounds. *Nat. Mater.* **2**, 587 (2003).

Supplementary Material

Supplementary materials can be viewed in this issue of the *Journal of Materials Research* by visiting http://journals.cambridge.org/jmr.

https://doi.org/10.1557/jmr.2013.255 Published online by Cambridge University Press